



HAL
open science

Metamaterial-Based LTCC Compressed Luneburg Lens Antenna at 60 GHz for Wireless Communications

Dmitry Zelenchuk, Vitalii Kirillov, Camilla Kärnfelt, François Gallée, Irina Munina

► **To cite this version:**

Dmitry Zelenchuk, Vitalii Kirillov, Camilla Kärnfelt, François Gallée, Irina Munina. Metamaterial-Based LTCC Compressed Luneburg Lens Antenna at 60 GHz for Wireless Communications. *Electronics*, 2023, 12 (11), pp.2354. 10.3390/electronics12112354 . hal-04112273

HAL Id: hal-04112273

<https://imt-atlantique.hal.science/hal-04112273v1>

Submitted on 31 May 2023

HAL is a multi-disciplinary open access archive for the deposit and dissemination of scientific research documents, whether they are published or not. The documents may come from teaching and research institutions in France or abroad, or from public or private research centers.




L'archive ouverte pluridisciplinaire **HAL**, est destinée au dépôt et à la diffusion de documents scientifiques de niveau recherche, publiés ou non, émanant des établissements d'enseignement et de recherche français ou étrangers, des laboratoires publics ou privés.



Distributed under a Creative Commons Attribution 4.0 International License

Article

Metamaterial-Based LTCC Compressed Luneburg Lens Antenna at 60 GHz for Wireless Communications

Dmitry Zelenchuk ^{1,*} , Vitalii Kirillov ² , Camilla Kärnfelt ³ , Francois Gallée ³ and Irina Munina ⁴¹ Centre for Wireless Innovations, Queen's University of Belfast, Belfast BT3 9DT, UK² Tyndall National Institute, T12 R5CP Cork, Ireland; vitalii.kirillov@tyndall.ie³ Lab-STICC, IMT Atlantique, UMR CNRS 6285, 29238 Brest, France; camilla.karnfelt@imt-atlantique.fr (C.K.); francois.gallee@imt-atlantique.fr (F.G.)⁴ Department of Mechanical, Manufacturing & Biomedical Engineering, Trinity College Dublin, D02 KF66 Dublin, Ireland; muninai@tcd.ie

* Correspondence: d.zelenchuk@qub.ac.uk

Abstract: In this study, a metamaterial-based LTCC compressed Luneburg lens was designed, manufactured and measured. The lens was designed at 60 GHz to utilize the unlicensed mm-wave spectrum available for short-range high-capacity wireless communication networks. The transformation optics method was applied to ensure the compression of the Luneburg lens antenna and thus maintain a low-profile structure. The two different types of unit cells for low and high permittivity regions were considered. The parametric study of the effect of compression on lens performance was presented. The antenna is implemented with a standard high-permittivity LTCC process, and details of the manufacturing process for the metamaterial lens are discussed. The low-profile lens is thinner than 2 mm and measures 19 mm in diameter. A size reduction of 63.6% in comparison with a spherical lens was achieved. The near-field to far-field mm-wave measurement technique is presented, and the measurement results show a peak antenna gain of 16 dBi at 60 GHz and a beam-scanning capacity with 1 dB scan loss within a 50° field of view.

Keywords: antenna; lens; metamaterial; mm-wave

Citation: Zelenchuk, D.; Kirillov, V.; Kärnfelt, C.; Gallée, F.; Munina, I. Metamaterial-Based LTCC Compressed Luneburg Lens Antenna at 60 GHz for Wireless Communications. *Electronics* **2023**, *12*, 2354. <https://doi.org/10.3390/electronics12112354>

Academic Editor: Dimitra I. Kaklamani

Received: 15 April 2023

Revised: 13 May 2023

Accepted: 17 May 2023

Published: 23 May 2023



Copyright: © 2023 by the authors. Licensee MDPI, Basel, Switzerland. This article is an open access article distributed under the terms and conditions of the Creative Commons Attribution (CC BY) license (<https://creativecommons.org/licenses/by/4.0/>).

1. Introduction

Nowadays, the demands on high-data-rate transmission are growing with the advance of modern wireless communications systems to 5G and beyond [1]. The wider use of the mm-wave spectrum has been proposed to increase the bandwidth as well as the spatial diversity to employ available propagation channels more efficiently [2]. Of particular interest is an unlicensed spectrum around 60 GHz that enables high-data-rate communications for multiple consumer applications [3]. This band is characterized by high path loss and the blocking of transmission losses by ordinary objects. This, in turn, leads to the requirements of high gain and beam steering capability of antenna systems to ensure the efficient operation of wireless networks [4].

Considering various candidate technologies such as printed circuit antenna arrays [5] and reflector antennas [6], some of the lens antennas stand out as solutions that offer natural beamforming properties with large radiation aperture resulting in a high gain [7].

The existing types of lenses for microwave applications vary from homogeneous dielectric lenses [7,8] to gradient-index lenses [9]. A widely known example of the latter is a Luneburg lens antenna, which has drawn the attention of researchers for enabling multibeam performance without scan loss within a wide field of view [10]. Such an antenna can be realized in a fully spherical shape or in a compressed form [11].

The compressed Luneburg lens is designed using a transformation optics approach and has been realized in X-band with a set of ceramic shapes [12] as well as by an assembly of stacked multilayer printed circuit boards [13] or by using a 3D printing technique [14].

In this paper, we address the challenge of building a solid metamaterial-based lens at 60 GHz. The low-temperature co-fired ceramics (LTCC) process is employed to ensure the appropriate tolerance and robustness of implementing a compressed Luneburg lens antenna operating at 60 GHz. The LTCC process allows further integration of the lens in an antenna-in-package solution and is of great interest for such lens antenna development.

The initial theoretical development of the structure was presented in [15]. The main contributions of this paper are summarized as follows:

- The paper significantly expands the design study by including a parametrical analysis of various aspects of the compressed lens and their effect on the LTCC lens performance.
- This paper presents details of the manufacturing of the LTCC lens and low-permittivity metamaterials in particular.
- A novel method of the near-field measurements of the 60 GHz lens is presented in the paper.
- Measurement results that verify the initial theoretical design proposed in [15] are also presented in this paper.

The paper is organized as follows: Section 2 discusses details of the compressed Luneburg lens antenna design in the LTCC process, Section 3 explores the compressed Luneburg lens antenna characteristics through full-wave simulations; Section 4 covers the fabrication aspects and Section 5 discusses the measurement techniques and results.

2. LTCC Compressed Luneburg Lens Design

The spherical Luneburg lens is a gradient index lens with relative permittivity varying radially as described by [16]:

$$\epsilon_r(r) = 2 - \left(\frac{r}{R}\right)^2 \quad (1)$$

where R is the lens radius and r is the radial position inside the lens (see Figure 1a).

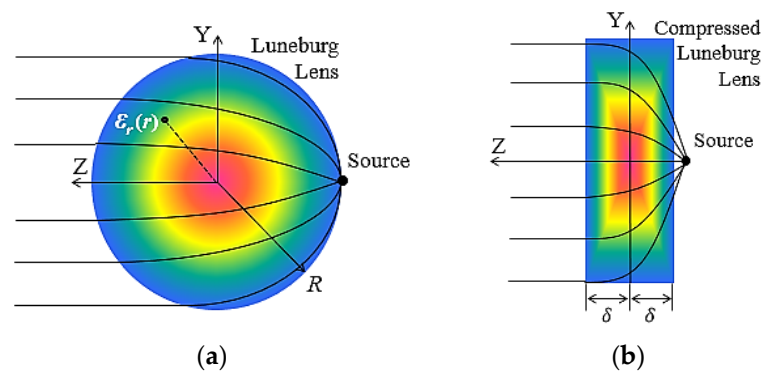


Figure 1. Spherical Luneburg lens (a) and compressed Luneburg lens (b).

In order to reduce the volume of the lens and make it more compatible with various types of feeding antennas and integrated electronics, the use of the transformation optics method has been proposed, and the lens was either partially or fully transformed to a cylindrical shape with a flat surface [10,12,17,18]. In this paper, we use the geometrical transformation presented in [12,18] to implement a compressed Luneburg lens as shown in Figure 1b. Note that full transformation leads to a 3×3 tensor as described in [18] and that further simplifications can be applied at the implementation stage based on the polarization:

$$y' = y, z' = \frac{\delta}{\sqrt{R^2 - y^2}} z \quad (2)$$

where δ is the half of the thickness of the compressed lens.

Applying the equations of transformation optics, one can calculate the permittivity and permeability distributions across the flat Luneburg lens [12,18]:

$$\begin{aligned} \epsilon' &= \left(2 - \frac{(R^2 - y'^2)z'^2 + (\delta y')^2}{(\delta R)^2} \right) \cdot \left| \sqrt{R^2 - y'^2} \right| \cdot \begin{pmatrix} A & B \\ B & \frac{1}{\delta} \end{pmatrix} \\ \mu' &= \left| \sqrt{R^2 - y'^2} \right| \cdot \begin{pmatrix} A & B \\ B & \frac{1}{\delta} \end{pmatrix} \end{aligned} \tag{3}$$

where coefficients A and B are defined as follows:

$$A = \frac{\delta(R^2 - y'^2) + \delta z'^2 y'^2}{(R^2 - y'^2)^3}, \quad B = \frac{z' y'}{\left| \sqrt{R^2 - y'^2} \right| (R^2 - y'^2)} \tag{4}$$

Based on the observations in [12,13,18], it has been shown that we can consider only the ϵ_{yy} or ϵ_{xx} element of the full tensor for TM- or TE-polarization, respectively.

In our case, for a flat Luneburg lens with radius $R = 9.5$ mm and compressed thickness $2\delta = 1.92$ mm, the permittivity distribution for ϵ_{yy} was calculated as shown in Figure 2. It can be seen that permittivity varies from 2 to 20.

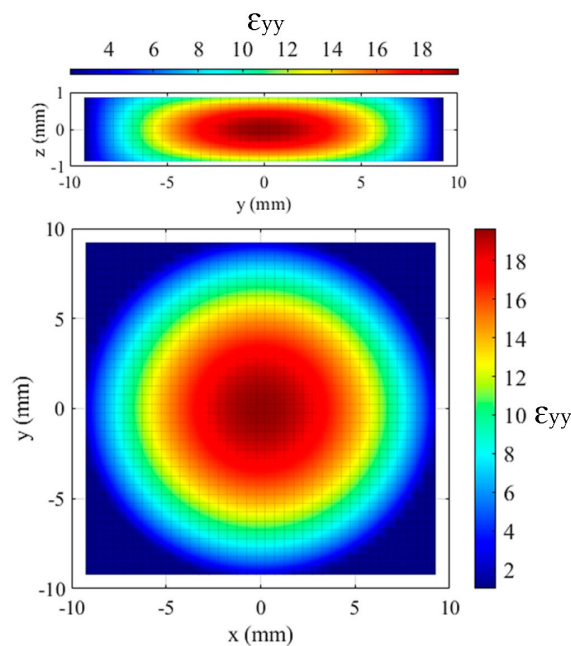


Figure 2. 2D cut of the distribution of permittivity ϵ_{yy} for the compressed Luneburg lens. $y = 0$ plane (top); $z = 0$ plane (bottom).

The lens was designed to be implemented with the LTCC process with the host material Ferro A6M-E of $\epsilon_r = 5.9$, loss tangent of 0.002 and layer thickness of 0.096 mm. In order to achieve the permittivity variation shown in Figure 2, two types of unit cells with a period of 0.5 mm and thickness 0.192 mm were implemented (see Figure 3). To obtain permittivity lower than 5.9, the unit cell was designed as a brick of the host material with a cylindrical hole, as shown in Figure 3a. The increase in the diameter of the hole leads to a reduction in the effective permittivity of the unit cell.

To realize high permittivity values, a unit cell with a rectangular metal patch was utilized (Figure 3b). The effective permittivity for both unit cells obtained with CST Microwave Studio is shown in Figure 4. Minimal hole and patch dimensions of 0.1mm were kept to comply with the manufacturing process and to reduce the impact of the tolerance of the process on the performance of the manufactured lens.

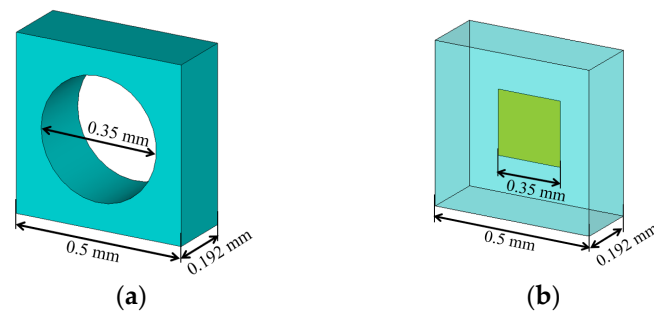


Figure 3. Metamaterial unit cells: (a) low permittivity, (b) high permittivity.

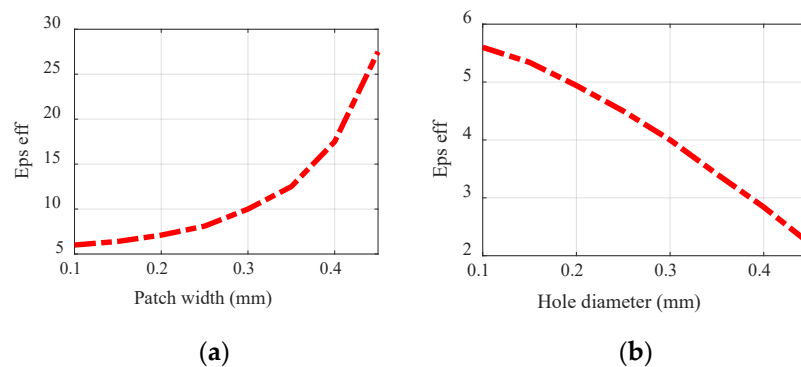


Figure 4. The permittivity of the metamaterial (a) vs. patch width; (b) vs. the hole diameter.

Finally, the model for the LTCC Luneburg lens was assembled in CST Microwave Studio (see Figure 5). One can see that most of the structure is composed of patch unit cells with the hole unit cells occupying a small area close to the outer surface of the lens. The dimensions of each patch and hole were chosen using data in Figure 4 to realize the permittivity distribution in (3).

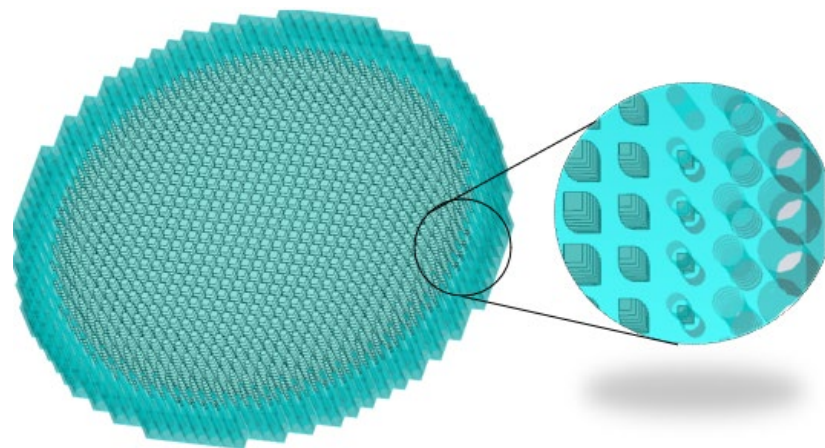


Figure 5. LTCC metamaterial Luneburg Lens.

It has been noted elsewhere [18] that for the compressed lens, the optimal focus is not at the surface of the lens but must be found empirically. In [19], simulated results of directivity for different positions of the feeding patch antenna on an optical axis were presented. Recently, [20] proposed a corrected approximation of the transformation optics for the metamaterial Luneburg lens that allows the placing of the focus of the compressed lens on the surface. The unit cell proposed in [20] is rather complex due to the necessity to correctly approximate the full permittivity tensor. In our work, we used a simplified formulation from [18] that allows the utilization of simpler unit cells, which is a more reliable and

repeatable approach for manufacturing mm-wave metamaterials. This approach resulted in the focus outside of the lens, which was thoroughly investigated. Analysis of this topic as well as lens simulation results are presented in the next section.

3. EM Simulations

In this section, we perform a parametric study of the focal distance as well as the effect of the compression on the lens performance. The first step was to feed the lens with a plane wave to find the focal point. The simulations were carried out at 60 GHz with CST Microwave Studio.

The focal distance was defined as the distance between the center of the lens and the point with the maximum magnitude of the electric field along the optical axis of the lens. The compression factor was changed by varying the number of the unit cells N_z along the principal axis of the lens, by taking into account that

$$N_z = \frac{2\delta}{h} \quad (5)$$

where h is the thickness of a unit cell and δ is half of the lens thickness. In the simulations, h equals to 0.192 mm, which corresponds to two LTCC layers with a thickness of 0.096 mm.

Figure 6 shows the results of the plane wave simulations. It is demonstrated that the focal distance decreases with the number of layers. The nonlinear dependence manifests a larger deviation of the focal point from the lens surface for a higher compression of the lens. Further increasing the number of layers has been found to be infeasible as this would exceed the limitations set by the available in-house manufacturing process (for our facilities, maximum $N_z = 10$).

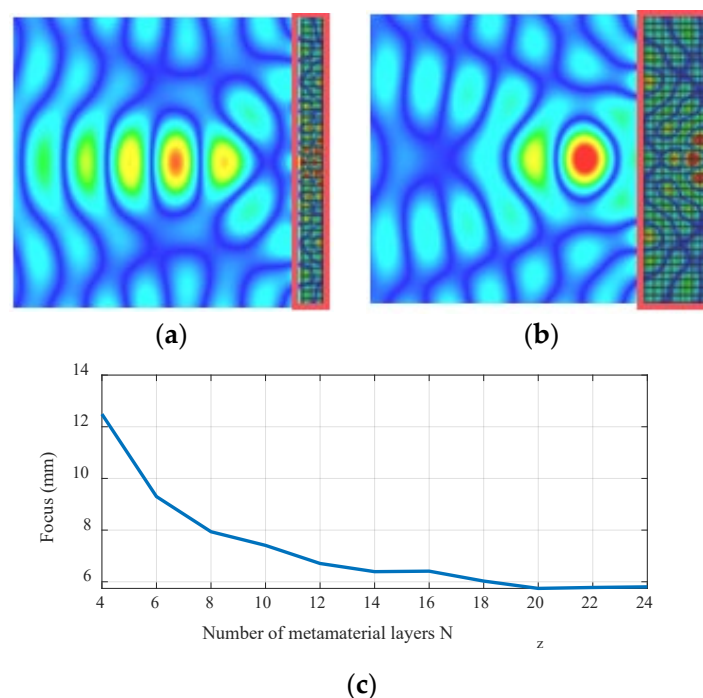


Figure 6. Simulated E-field distribution for the lens (red rectangular) with $N_z = 8$ (a) and the lens with $N_z = 22$ (b). Focal distance vs. the number of layers (c).

Another set of simulations was carried out by feeding the lens with an open-ended waveguide (OEWG) with a cross-section of 1.55×3.1 mm. The distance to the feed and its lateral displacement are shown in Figure 7. The lens on its own is broadband. Reflection coefficient bandwidth is defined only by the type of the feed. In our case, it corresponds to the OEWG.

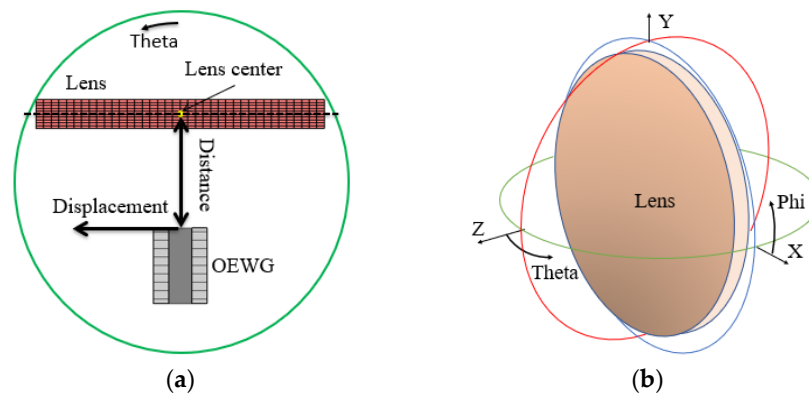


Figure 7. (a) Top view of cross-section of the simulated model. (b) Angle explanation of angular coordinates: ZOY—theta green plane when phi = 0; ZOY—theta red plane when phi = 90, XOY—blue plane).

The dependence of the gain on the number of unit cells and the distance to the feed are shown in Figure 8. In our simulations, we used the realized gain as the metric that incorporates the effect of impedance matching as well. It can be seen that for the different numbers of unit cells in the lens structure, the optimal position of the feed changes. An increasing number of unit cell lenses leads to the position of the feed being closer to its surface. For instance, with an 8-layer lens, the distance to the feed is 9 mm; the same gain can be obtained with a 22-layer lens and a 5 mm distance to the feed. The simulations support our previous finding that the focal point moves away from the lens surface for lenses with higher compression.

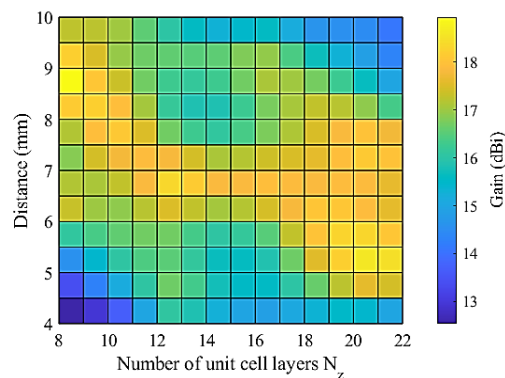


Figure 8. Gain as a function of the number of unit cells N_z and distance to the feed without OEWG displacement.

The beam steering capability in such lens antenna systems is obtained by shifting the OEWG. This displacement leads to additional gain reduction due to inefficient illumination of the lens surface. To estimate the gain, simulations for the lens with the number of unit cell layers $N_z = 10$ with different displacements of the OEWG were carried out. Figure 9 shows gain as a function of the OEWG shift along the optical axis of the lens (distance to the feed) and laterally (displacement of the feed). One can see that in order to effectively illuminate the surface of the compressed lens, it is necessary to increase the distance to the feed when the feed is laterally displaced.

In our case, a focus of 5.96 mm (where 0.96 mm is half the lens thickness and 5 mm is the distance between the lens surface and the OEWG) was chosen. Taking into account that in the case of a spherical lens, the focus is equal to its radius, an approximately 63.6% size reduction was achieved in our lens antenna system. Radiation pattern results for this focal distance and different OEWG displacements are presented in Figure 10. In comparison with the OEWG without the lens, the antenna gain was enhanced by 11 dB to 16.8 dBi.

In this particular case, the sidelobe level was 15 dB for a 0 mm OEWG displacement and around 10 dB for an OEWG laterally shifted by 5 mm. In addition, shifting the waveguide with a 2.5 mm step allowed overlapping radiation patterns at -2 dB level. Beamwidth and gain as a function of frequency are shown in Figure 11. Since a lens is a wideband device, its gain increases with frequency, and a compressed lens exhibits the same tendency. The impedance matching mostly corresponded to one of the exciting waveguides and the return loss was better than 10 dB across the simulated frequency band (56–64 GHz).

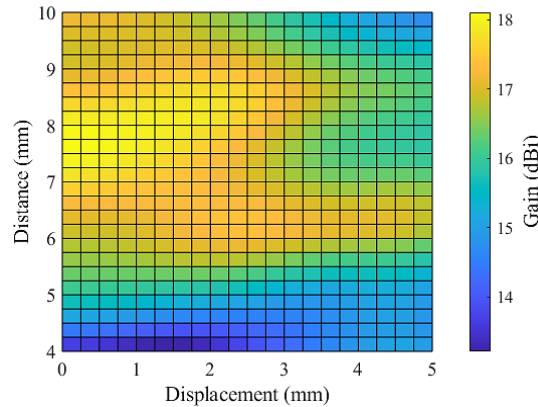


Figure 9. Gain as a function of the OEWG shift along the optical axis of the lens (distance to the feed) and laterally (displacement of the feed) for the lens with $N_z = 10$.

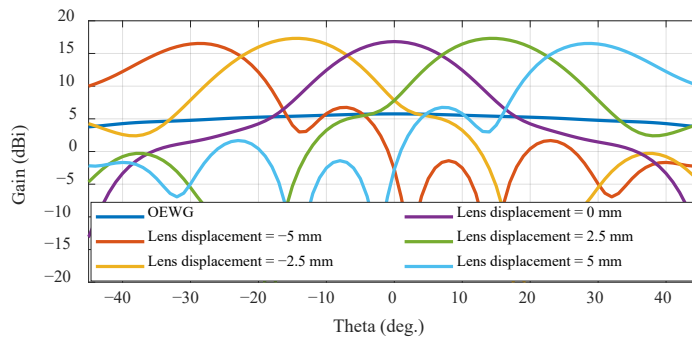
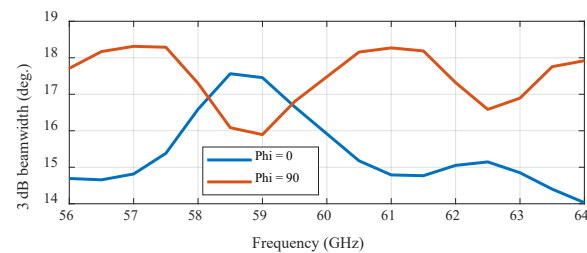
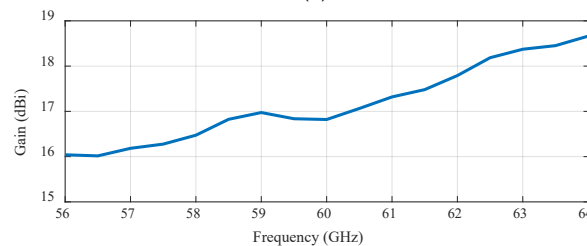


Figure 10. Simulated gain for Luneburg lens with open-ended waveguide excitation at 60 GHz.



(a)



(b)

Figure 11. Simulated beamwidth (a) and gain (b) as a function of frequency for a Luneburg lens with open-ended waveguide excitation.

4. Lens Fabrication

The Luneburg lens is fabricated in-house. All twenty layers were laser-cut to create the alignment holes and the metamaterial holes along the periphery of the lens radius. The metamaterial holes differ a little in diameter and position for every layer even though perfect symmetry is kept in the z-direction. The layer count starting at the bottom layer is 1A, 1B, 2A, 2B, to 10B, which is the top layer. The metamaterial pattern is radially symmetric, and a z-direction symmetry is obtained with its center at the intersection between layers 5B and 6A. The hole pattern of layers 1A and 1B is precisely the same as for layers 10A and 10B, respectively; likewise for layers 2A and 2B and layers 9A and 9B, etc. The same goes for the screen-printed metamaterial patches, where the same pattern is used on layers 1A and 10A, 2A and 9A and so forth. Ferro gold paste CN30-080M is used. No screen printing is performed on the B layers. All layers are presented in Figure 12. Details of a layer pair are given in Figure 13. As can be seen, the laser-cut holes of these two layers are the same. When stacked, the patches are located in the center of every layer pair.

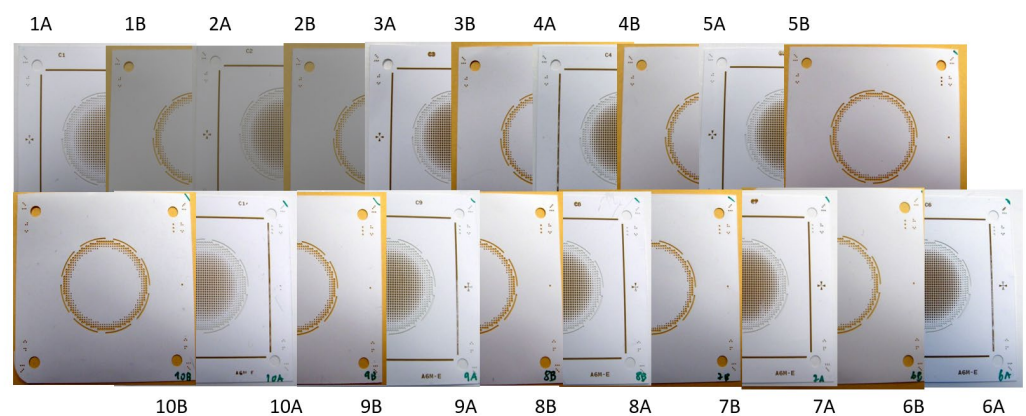


Figure 12. The 20 layers after laser cutting and screen printing, placed in their stacking order from 1A (bottom) to 10B (top).

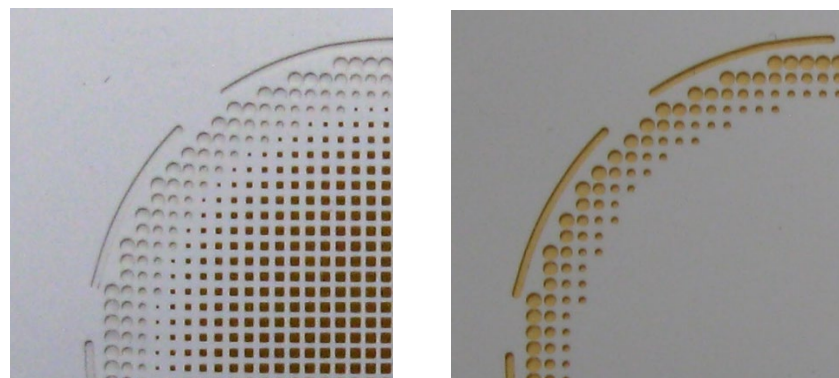


Figure 13. Details of a layer pair, in this example, for 1A (left) and 1B (right). The cut holes for each layer pair are the same. After stacking, the screen-printed patches are found between the two dielectric layers.

After preparing the layers, stacking was made with the help of an alignment fixture, (see Figure 14). For each stacked layer, HEC 2wt% (Hydroxyethyl-cellulose) was filled in the holes manually by using a spatula. This HEC material serves to protect the holes from collapsing during lamination. The method has been published in [21]. After stacking, uniaxial lamination was performed at 70 °C with an applied pressure of 17 MPa for 5 min. Then, the lens was separated from the rest of the LTCC by laser. The last fabrication step was the firing at 850 °C peak temperature for 30 min. The finalized antenna is presented in Figure 15. Some damage can be seen at the outer periphery of the lens. This may have some impact on the measured results.

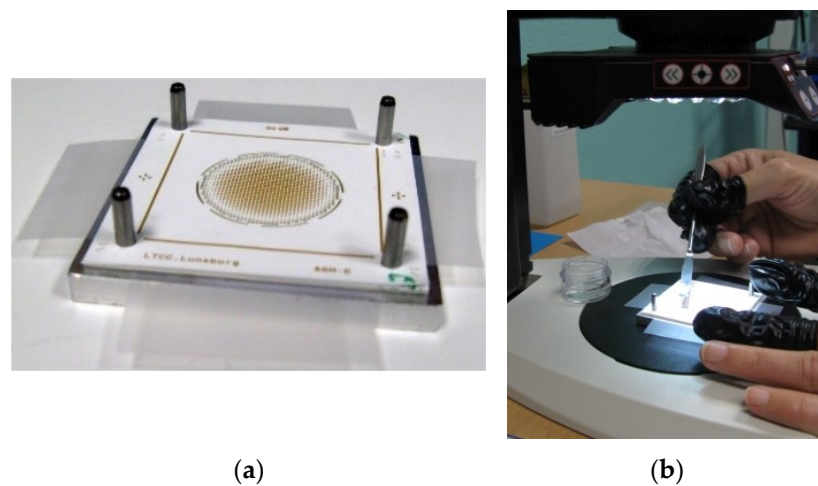


Figure 14. Stacking procedure. (a) Alignment of layers is done with the help of a fixture. (b) Filling of metamaterial holes by HEC 2wt% on each layer.

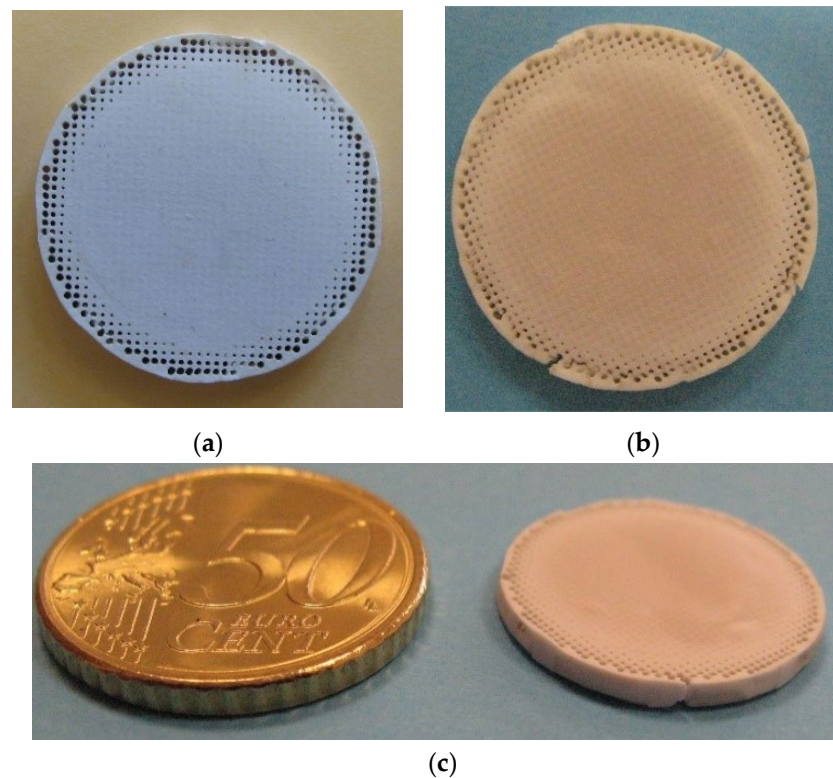


Figure 15. Finalized lens antenna (a) before firing, and (b) after firing. (c) The lens sample in comparison with a 50-euro-cent coin.

5. Measurements

The measurement setup was based on a spatial scan with a 6-axis robot. The OEWG is connected to an RF generator, SMA100B, with an external multiplier to generate the 60 GHz. The RX probe, fixed to the arm of the robot, consists of a horn antenna with a harmonic mixer connected to an R&S FSV3000 spectrum analyzer. The measured 3D radiation pattern is calculated from planar scans in the near-field region. Only the magnitude measurement is performed. The phase distribution is then computed by applying an iterative Fourier Technic (IFT) from the measurement on two layers [22]. The principle of phase extraction is shown in Figure 16.

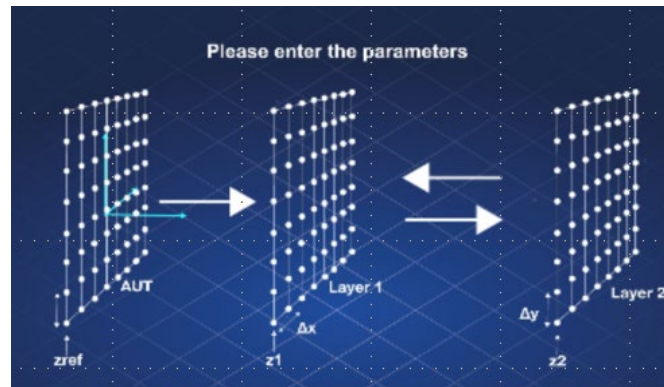
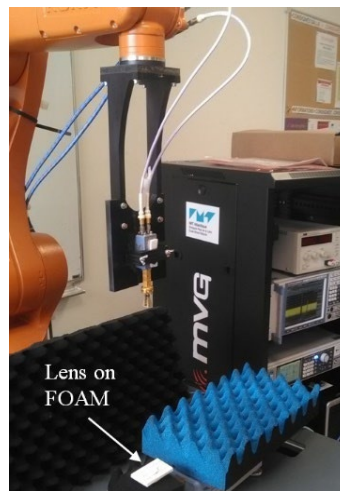
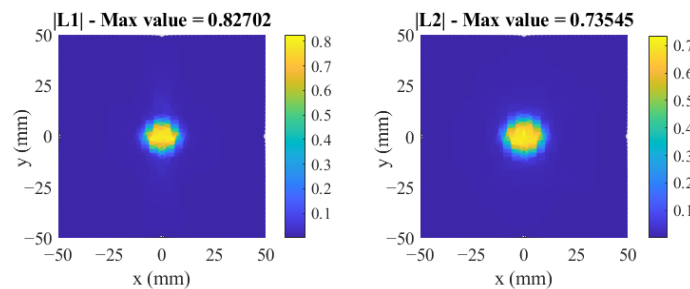


Figure 16. Principle of extraction of the phase distribution.

Measurements were carried out by feeding the lens with the OEWG through a piece of foam with 5 mm thickness, as shown in Figure 17a. Two 100 × 100 mm planes are scanned above the lens at different heights. Figure 17b shows the magnitude distribution of the electric field on the two layers at 1 mm and 15 mm above the lens, and the phase distribution is then computed from the IFT.



(a)



(b)

Figure 17. (a) Measurement setup. (b) Electric field measurement on the layers L1 (10 mm) and L2 (15 mm) above the lens.

The measured 3D radiation pattern is computed from a classic near-field to far-field transformation available in Altair FEKO Software and is shown in Figure 18. To analyze the scanning performance, the probe is moved along the 200 mm circle with a center at the top of the lens opposite the OEWG center. The radiation pattern was measured in the range between -45° and 45° for the Luneburg lens as well as the OEWG at 60 GHz, as shown in

Figure 19. It can be seen that the lens provides a 10 dB gain enhancement in comparison to the OEWG. The side lobe level for this sample is defined as 10 dB. By moving the OEWG along the lens, beam-steering capability is achieved. We can see from the measurements that a 5 mm shift of the feed leads to beam steering at 25 degrees with 1 dB scan loss. The total gain was measured and compared to the simulation in Figure 19c. The broadside gain of the manufactured lens antenna was equal to 16 dBi at 60 GHz. Radiation efficiency of 89% and aperture efficiency of 28% were calculated at 60 GHz. The latter figure is explained by the non-optimal illumination of the lens area, which is reasonable as the source is moved across the surface of the lens to achieve beam steering.

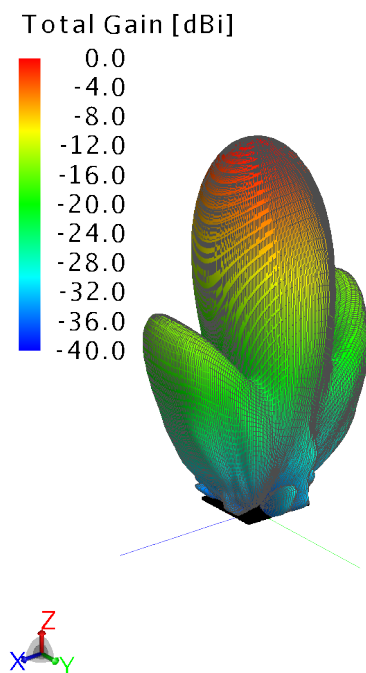


Figure 18. Measured 3D radiation pattern.

Table 1 summarizes the key features of the LTCC-compressed lens and several comparable V-band lens antennas that aim for high-gain performance with the potential for multibeam or beam-steering operation. A 3D-printed 60 GHz Luneburg lens based on the infill density of the plastic is demonstrated in [23]. A solid hemispherical plastic lens printed for integration with a transceiver was developed in [24]. A molded plastic elliptical lens with circular waveguide feed and mechanical beam steering capacity was demonstrated in [25]. A 3D-printed dielectric Fresnel-Zone Plate Lens (FZPL) antenna for use within the V-band spectrum is presented in [26]. As per the table, the proposed lens operates on the same frequency range and exhibits comparable performance to other lenses. However, its reported size is considerably smaller, resulting in a notable impact on the overall antenna system size. This reduction in size could potentially lead to a more compact and efficient antenna design, making it a promising option for various applications.

Table 1. Different V-band lens solutions.

Ref.	Lens Type	Gain (dBi)	Size in λ at f_0	f_0 (GHz)
[23]	3D printed	15.3	$6 \times 6 \times 6$	60
[24]	3D printed	14	$3 \times 3 \times 2.9$	60
[25]	Molded plastic	14	$4 \times 4 \times 4.36$	62.5
[26]	3D printed	25	$30 \times 30 \times 1$	60
This work	LTCC metamaterial	15	$3.8 \times 3.8 \times 0.384$	60

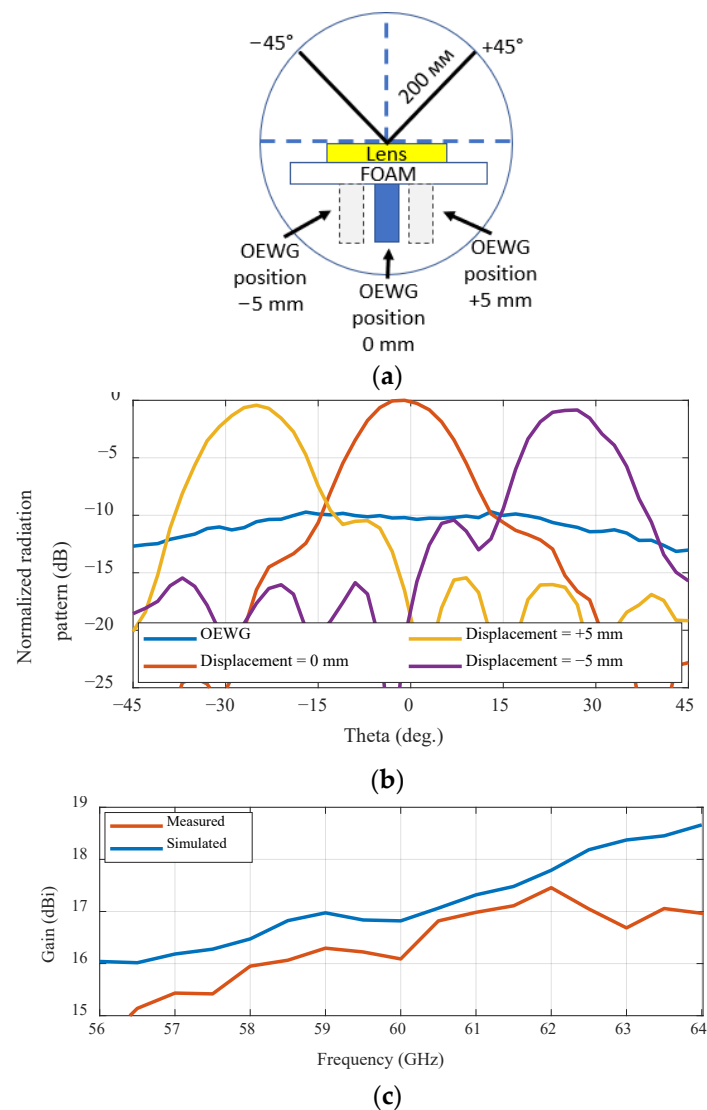


Figure 19. Detailed sketch of the lens position (a), the measured radiation pattern of the Luneburg lens and the standalone open-ended waveguide (b), and comparison of the simulated and measured broadside gain vs. frequency (c).

6. Conclusions

A 60 GHz metamaterial compressed Luneburg lens designed compatible with the LTCC process has been proposed in this paper. The effect of the compression on the focal point as well as the performance of the lens fed by a laterally displaced OEWG was studied. It was shown that the focal point is placed outside the lens and depends on the number of LTCC layers. The gain of the lens is shown to be a function of the thickness of the compressed lens. It was also shown that the scan loss of 1 dB can be achieved within a 50° field of view with a maximum gain of 16.8 dBi.

The lens was manufactured using an in-house LTCC process and measured at 60 GHz using two-plane near-field scanning and a subsequent iterative IFT method. The measured results are in good agreement with the simulation, with a 16 dBi maximum gain at 60 GHz and 1dB scan loss achieved.

The LTCC process allows further integration of control elements and active circuitry to make use of the lens in a multi-beam standalone transceiver for mm-wave communications that will be explored in future work.

Author Contributions: Conceptualization, D.Z., C.K. and F.G.; design methodology, software and investigation, D.Z., I.M. and V.K.; LTCC design and manufacturing, C.K.; measurement methodology, validation and visualization, F.G.; writing—original draft preparation, writing—review and editing, all the authors; funding acquisition, D.Z., I.M., C.K. and F.G. All authors have read and agreed to the published version of the manuscript.

Funding: This research was partially funded by the Department for the Economy of Northern Ireland under US Ireland R&D Partnership grant no. USI 199, EPSRC EP/S007954/1 and the EU Horizon 2020 under the Marie Skłodowska-Curie grant agreement No. 847402. Contributions to the equipment were given by the European Union through the European Fund for Economic and Regional Development (FEDER), the Ministry of Education, Higher Education and Research, the Region of Brittany and Brest Metropole through the CPER project “SOPHIE/STIC & Ondes” and the “Fonds de Concours à la Recherche” (FCR2019) as well as the Departmental Council of Finistère through the Aid to Emerging Research Programs (AAPRE) and the Carnot funds.

Data Availability Statement: The data presented in this study are available on request from the corresponding author.

Conflicts of Interest: The authors declare no conflict of interest.

References

1. Hong, W.; Jiang, Z.H.; Yu, C.; Hou, D.; Wang, H.; Guo, C.; Hu, Y.; Kuai, L.; Yu, Y.; Jiang, Z.; et al. The Role of Millimeter-Wave Technologies in 5G/6G Wireless Communications. *IEEE J. Microw.* **2021**, *1*, 101–122. [[CrossRef](#)]
2. Niu, Y.; Li, Y.; Chen, S.; Jin, S.; Qiu, L. A Survey of Millimeter Wave Communications (MmWave) for 5G: Opportunities and Challenges. *Wirel. Netw.* **2015**, *21*, 2657–2676. [[CrossRef](#)]
3. Boccardi, F.; Heath, R.W.; Lozano, A.; Marzetta, T.L.; Popovski, P. Five Disruptive Technology Directions for 5G. *IEEE Commun. Mag.* **2014**, *52*, 74–80. [[CrossRef](#)]
4. Imbert, M.; Romeu, J.; Baquero-Escudero, M.; Martinez-Ingles, M.-T.; Molina-Garcia-Pardo, J.-M.; Jofre, L. Assessment of LTCC-Based Dielectric Flat Lens Antennas and Switched-Beam Arrays for Future 5G Millimeter-Wave Communication Systems. *IEEE Trans. Antennas Propag.* **2017**, *65*, 6453–6473. [[CrossRef](#)]
5. Jouanlanne, C.; Clemente, A.; Huchard, M.; Keignart, J.; Barbier, C.; Nadan, T.L.; Petit, L. Wideband Linearly Polarized Transmitarray Antenna for 60 GHz Backhauling. *IEEE Trans. Antennas Propag.* **2017**, *65*, 1440–1445. [[CrossRef](#)]
6. Alfonso, E.; Kildal, P.-S. Parabolic Cylindrical Reflector Antenna at 60 GHz with Line Feed in Gap Waveguide Technology. In Proceedings of the 7th EuCAP, Gothenburg, Sweden, 8–12 April 2013; pp. 8–12.
7. Ansarudin, F.; Rahman, T.A.; Yamada, Y.; Rahman, N.H.A.; Kamardin, K. Multi Beam Dielectric Lens Antenna for 5G Base Station. *Sensors* **2020**, *20*, 5849. [[CrossRef](#)] [[PubMed](#)]
8. Pivit, F.; Doumanis, E.; Kozlov, D.; Gueye, M.; Gimersky, M. Compact 60-GHz Lens Antenna with Self-Alignment Feature for Small Cell Backhaul. In Proceedings of the 2017 IEEE-APS Topical Conference on Antennas and Propagation in Wireless Communications (APWC), Verona, Italy, 11–15 September 2017; pp. 280–283.
9. Larimore, Z.; Jensen, S.; Good, A.; Lu, A.; Suarez, J.; Mirotznik, M. Additive Manufacturing of Luneburg Lens Antennas Using Space-Filling Curves and Fused Filament Fabrication. *IEEE Trans. Antennas Propag.* **2018**, *66*, 2818–2827. [[CrossRef](#)]
10. Biswas, S.; Lu, A.; Larimore, Z.; Parsons, P.; Good, A.; Hudak, N.; Garrett, B.; Suarez, J.; Mirotznik, M.S. Realization of Modified Luneburg Lens Antenna Using Quasi-conformal Transformation Optics and Additive Manufacturing. *Microw. Opt. Technol. Lett.* **2019**, *61*, 1022–1029. [[CrossRef](#)]
11. Gao, J.; Wang, C.; Zhang, K.; Hao, Y.; Wu, Q. Beam Steering Performance of Compressed Luneburg Lens Based on Transformation Optics. *Results Phys.* **2018**, *9*, 570–575. [[CrossRef](#)]
12. Mateo-Segura, C.; Dyke, A.; Dyke, H.; Haq, S.; Hao, Y. Flat Luneburg Lens via Transformation Optics for Directive Antenna Applications. *IEEE Trans. Antennas Propag.* **2014**, *62*, 1945–1953. [[CrossRef](#)]
13. Su, Y.; Chen, Z.N.; Skrivervik, A.K. A Compact Transformation Optics-Based Luneburg Lens Antenna Using Curved Reactive Impedance Surface. In Proceedings of the 2021 15th European Conference on Antennas and Propagation (EuCAP), Dusseldorf, Germany, 22–26 March 2021; pp. 1–4.
14. Giddens, H.; Andy, A.S.; Hao, Y. Multimaterial 3-D Printed Compressed Luneburg Lens for Mm-Wave Beam Steering. *IEEE Antennas Wirel. Propag. Lett.* **2021**, *20*, 2166–2170. [[CrossRef](#)]
15. Zelenchuk, D.; Karnfelt, C.; Gallee, F.; Munina, I. Metamaterial-Based LTCC Compressed Luneburg Lens Antenna at 60 GHz for Wireless Communications. In Proceedings of the 2021 IEEE International Conference on Microwaves, Antennas, Communications and Electronic Systems (COMCAS), Tel Aviv, Israel, 1–3 November 2021; pp. 513–515.
16. Luneburg, R.K.; King, A.L. Mathematical Theory of Optics. *Am. J. Phys.* **1966**, *34*, 80–81. [[CrossRef](#)]
17. Kadera, P.; Sanchez-Pastor, J.; Eskandari, H.; Tyc, T.; Sakaki, M.; Schusler, M.; Jakoby, R.; Benson, N.; Jimenez-Saez, A.; Lacik, J. Wide-Angle Ceramic Retroreflective Luneburg Lens Based on Quasi-Conformal Transformation Optics for Mm-Wave Indoor Localization. *IEEE Access* **2022**, *10*, 41097–41111. [[CrossRef](#)]

18. Su, Y.; Chen, Z.N. A Flat Dual-Polarized Transformation-Optics Beamscanning Luneburg Lens Antenna Using PCB-Stacked Gradient Index Metamaterials. *IEEE Trans. Antennas Propag.* **2018**, *66*, 5088–5097. [[CrossRef](#)]
19. Demetriadou, A.; Hao, Y. Slim Luneburg Lens for Antenna Applications. *Opt. Express* **2011**, *19*, 19925. [[CrossRef](#)] [[PubMed](#)]
20. Xu, R.; Chen, Z.N. A Transformation-Optics-Based Flat Metamaterial Luneburg Lens Antenna With Zero Focal Length. *IEEE Trans. Antennas Propag.* **2022**, *70*, 3287–3296. [[CrossRef](#)]
21. Kärnfelt, C.; Zelenchuk, D.; Sinou, M.; Gallée, F.; Douglas, P. Sacrificial Volume Materials for Small Hole Generation in Low-Temperature Cofired Ceramics. *Electronics* **2020**, *9*, 2168. [[CrossRef](#)]
22. Capozzoli, A.; Curcio, C.; D’Elia, G.; Liseno, A. Phaseless Antenna Characterization by Effective Aperture Field and Data Representations. *IEEE Trans. Antennas Propag.* **2009**, *57*, 215–230. [[CrossRef](#)]
23. Norooziarab, M.; McCloskey, D.; Kozlov, D.S.; Kirillov, V.V.; Bulja, S.; Pivit, F.; Rulikowski, P. Millimeter-Wave 3D Printed Luneburg Lens Antenna. In Proceedings of the 2019 IEEE Radio and Antenna Days of the Indian Ocean (RADIO), Saint-Gilles, Belgium, 23–26 September 2019; pp. 1–2.
24. Bisognin, A.; Titz, D.; Ferrero, F.; Pilard, R.; Fernandes, C.A.; Costa, J.R.; Corre, C.; Calascibetta, P.; Riviere, J.-M.; Poulain, A.; et al. 3D Printed Plastic 60 GHz Lens: Enabling Innovative Millimeter Wave Antenna Solution and System. In Proceedings of the 2014 IEEE MTT-S International Microwave Symposium (IMS2014), Tampa, FL, USA, 1–6 June 2014; pp. 1–4.
25. Costa, J.R.; Lima, E.B.; Fernandes, C.A. Compact Beam-Steerable Lens Antenna for 60-GHz Wireless Communications. *IEEE Trans. Antennas Propag.* **2009**, *57*, 2926–2933. [[CrossRef](#)]
26. Pourahmadazar, J.; Denidni, T.A. Towards Millimeter-Wavelength: Transmission-Mode Fresnel-Zone Plate Lens Antennas Using Plastic Material Porosity Control in Homogeneous Medium. *Sci. Rep.* **2018**, *8*, 5300. [[CrossRef](#)] [[PubMed](#)]

Disclaimer/Publisher’s Note: The statements, opinions and data contained in all publications are solely those of the individual author(s) and contributor(s) and not of MDPI and/or the editor(s). MDPI and/or the editor(s) disclaim responsibility for any injury to people or property resulting from any ideas, methods, instructions or products referred to in the content.